Faint phase synchronization detection through structured orthomax rotations in singular spectrum analysis

Leonardo L. Portes [*]

Complex Systems Group, Department of Mathematics and Statistics, University of Western Australia, Nedlands, Perth, WA 6009, Australia

Michael Small

Complex Systems Group, Department of Mathematics and Statistics, University of Western Australia, Nedlands, Perth, WA 6009, Australia
and Mineral Resources, CSIRO, Kensington, Perth, WA 6151, Australia

Multivariate singular spectrum analysis (M-SSA), with a structured varimax rotation, is a method that allows a deep characterization of phase synchronization (PS) phenomena in an almost automatic fashion. It has been increasingly used in the study of PS in networks of nonlinear, real-world, and numeric systems. This paper investigates the impact of the other recently developed structured orthomax rotations on the M-SSA ability to characterize PS. The results show that by using the structured quartimax rotation, a very faint and intermittent PS regime can be detected, in contrast with the structured varimax (which demands a stronger, more consolidated PS regime). This is due to the fact that the different rotations do not have the same efficiency in achieving a simple structure of the M-SSA eigenvectors. Nevertheless, for well-established PS regimes, the same robustness of the original M-SSA approach against high levels of additive Gaussian noise was found for the structured quartimax and biquartimax rotations. However, for all approaches we found an overshoot of the qualitative range for the PS onset due to noise.

I. INTRODUCTION

Multivariate singular spectrum analysis (M-SSA) is a well-established method in the investigation of temporal and spatial patterns in diverse fields of science [1]. In this decade, the method was adapted to deal with the detection and characterization of chaotic phase synchronization (PS) in networks of nonlinear dynamical systems [2]. Under this scenario, the lack of a universal definition or estimate of phase or frequency was one of the main challenges. However, M-SSA is able to provide detailed information regarding the dynamics of PS, with no *a priori* need for a phase or frequency estimate. Nevertheless, this is achieved in a *automatic* fashion by detecting oscillatory modes present in data. This is made through the eigendecomposition of a concatenated trajectory matrix from the measured time series of the network oscillators. The sharing of oscillatory modes by different systems implies in the formation of PS clusters. This method has undergone intense development in recent years [3–7], and it has been applied in diverse natural [3,8,9] and numerical scenarios [10,11].

The efficiency of the method is largely due to the introduction of a specially crafted varimax rotation by Groth and Ghil [2]. Without this rotation, the M-SSA eigenvectors are not (pairwise) uniquely related to the oscillatory modes within the data, and hence no information of the underlying of PS clustering is provided. Recently, a closed-matrix formulation

for Groth and Ghil's *modified* varimax was developed [5], in which it was called a *structured* varimax (s-varimax), as contrasted to the classical Kaiser's varimax rotation [12]. Nonetheless, the authors in Ref. [5] extended this matrix approach to the entire family of *structured* orthomax (s-orthomax) rotation criteria by following a modern gradient projection approach [13,14]. It was shown as well that the advantage of the s-varimax over the classical one appears only when dealing with multimodal systems (specifically, this was shown through a numerical investigation with coupled Rösslers oscillators in the funnel or nonphase coherent chaotic regime).

Classical orthomax rotations were developed in the field of psychometrics. The underlying motivation was a better understanding of experimental outcomes in factor analysis by achieving a "simple structure" for a factor pattern matrix [15,16]. Kaiser's varimax is the most-efficient (orthogonal) rotation [17]. Hence it was just natural for Groth and Ghill to use the varimax as the basis for their structured (modified) orthogonal rotation to achieve a simple structure of the M-SSA eigenvectors in the analysis of PS. We make a systematic investigation of the s-orthomax rotations on the M-SSA technique, with a comparison with its standard application with the s-varimax.

The new findings of this study a fourfold. First, the M-SSA with the different s-orthomax rotations has different sensitivities for PS characterization. For example, a weak (or less developed, highly intermittent) PS regime can be detected by using the s-quartimax rotation but not with the s-varimax. Second, only three (of four) members of the s-orthomax

———————
[*]ll.portes@gmail.com

family are useful in characterizing synchronization. Specifically, the s-equamax criterion is not able to find a rotation to convey a simple structure of the M-SSA eigenvectors in the context of PS analysis. Third, the gradient projection algorithm [5] fails to achieve a suitable s-varimax rotation under the single-variable M-SSA approach [4] for two coupled systems. This is due to the fact that the s-varimax and the s-equamax are equivalent in *this* specific context, which explains why the authors in Ref. [4] empirically applied a different criterion from the strict s-varimax one. Finally, we show that the M-SSA PS onset characterization is not robust against additive Gaussian noise.

The M-SSA approach with the s-varimax, and the matrix extension to the s-orthomax family rotations, are briefly reviewed in Sec. II. The numerical experimental design and complementary analytical tools are presented in Sec. III. The results for the full multivariable approach [2] and single-variable approach [4] (with the best system observable) are shown and discussed in Sec. IV. Final remarks and prescriptions are presented in Sec. V.

II. BACKGROUND

A. M-SSA and the *structured* varimax

Here we briefly review the s-varimax M-SSA for chaotic PS analysis [2–4]. Consider $j = 1, \ldots, J$ coupled dynamical systems and the measured time series $\{s_d(i)\}_{i=1}^N$ at time i and with length N. Here $d = 1, \ldots, D$ is the number of channels, or time series, used to represent the systems. In the multivariable approach [2,3], any number of time series can be used to represent a given oscillator (e.g., the three time series from x, y, and z of the Rössler system). In the single-variable approach [4], only the time series from the best observable of each system is used, and then $D = J$. The M-SSA approach for the characterization of chaotic phase synchronization can be defined by the following steps:

(1) Build individual trajectory matrices $\mathbf{X}_d$ by embedding each (centered and normalized) $\{s_d(i)\}$ in an m-dimensional space with lag 1 [18,19] (m is also called window width).

(2) Construct the *augmented* trajectory matrix $\mathbf{X} = [\mathbf{X}_1, \ldots, \mathbf{X}_D] \in \mathrm{R}^{N-m+1, Dm}$, by concatenating the individual ones.

(3) Extract the "skeleton" of the structure encoded in the time series by performing a singular value decomposition of $\mathbf{X} = \mathbf{P\Lambda E}^T / (N - m + 1)^{1/2}$ or, equivalently, the eigendecomposition of the covariance matrix $\mathrm{cov}(\mathbf{X}) = \mathbf{X}^T \mathbf{X} / (N - m + 1)$ as $\mathrm{cov}(\mathbf{X}) = \mathbf{E\Sigma E}^T$.

(4) Perform the *structured* varimax rotation of the first S eigenvectors $\mathbf{E}_S^* = \mathbf{E}_S \mathbf{T}$, and compute the respective *modified* variances $\{\lambda_k^*\}_{k=1}^S \equiv \mathrm{diag}(\mathbf{\Lambda}_S^*)$ as $\mathbf{\Lambda}_S^* = \mathbf{T}^T \mathbf{\Lambda}_S \mathbf{T}$.

For an in-depth discussion, alternative procedures, and pitfalls regarding the spectrum decomposition, we refer the reader to Refs. [1,2].

Figure 1 provides an illustrative representation of the expected outcomes of this analysis for $J = 4$ coupled and detuned chaotic phase-coherent oscillators (the phase-coherence implies in a sharp, well-defined, intrinsic frequency. Then each oscillator has a single oscillatory mode which shall be represented as a pair of eigenvalues or eigenvectors in the
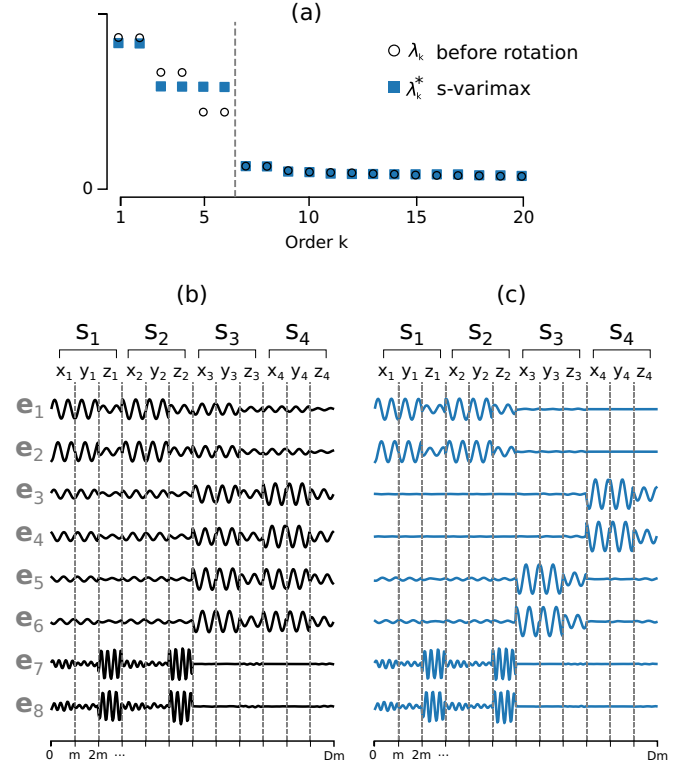

FIG. 1. Schematic representation of the multivariable M-SSA for $J = 4$ idealized coupled and detuned phase-coherent oscillators. The scenario in which oscillators $j = \{1, 2\}$ are phase synchronized (forming a PS cluster) is depicted. (a) Singular values $\lambda^{1/2}$ and associated eigenvectors (b) before and (c) after rotation. The s-varimax rotation is necessary to reveal the synchronized behavior (i.e., oscillatory mode sharing). The single-variable approach yields a qualitatively similar picture, but the eigenvectors in (b) and (c) would spam only one time series per system (e.g., only for $\{y_1, y_2, y_3, y_4\}$).

M-SSA). This example depicts a specific regime which oscillators $j = 1, 2$ are phase synchronized, while the remaining oscillators $j = 3, 4$ remains out of sync. The M-SSA operates in a way to identify the *shared oscillatory modes* within the data sets. Before the s-varimax rotation, no information of this shared structure is captured by neither the variances λ_k [black rings in Fig. 1(a)] or by the eigenvectors $\mathbf{e_k}$ [Fig. 1(b)].

Groth and Ghil's idea was to impose the "simple structure" on the eigenvector matrix $\mathbf{E}$ but not on each column (which would be the original Kaiser's varimax): Given the underlying structure of the augmented trajectory matrix $\mathbf{X}$ [see step 2, above, and Fig. 1(b)], the simple structure should be imposed on the D blocks (of length m) of each channel $d = 1, \ldots, D$. Hence, the matrix $\mathbf{E}$ should be rotated in a constrained fashion that respects its special *structure*. To achieve this, under an arbitrary orthogonal rotation $\mathbf{T}$, and defining the rotated vectors $\mathbf{E}^* = \mathbf{ET}$, Groth and Ghil proposed to first sum over the individual channels [2],

$$\bar{e}_{dk}^{*\,2} = \sum_{m=1}^M e_{dk}^{*\,2}(m), \tag{1}$$

and compute the simplicity Q over the new vectors $\bar{\mathbf{e}}_k^*$,

$$Q(\mathbf{ET}) = \frac{1}{D}\sum_{k=1}^{S}\left[\sum_{d=1}^{D}\left(\bar{e}_{dk}^{*2}\right)^2 - \frac{1}{D}\left(\sum_{d=1}^{D}\bar{e}_{dk}^{*2}\right)^2\right], \quad (2)$$

where S stands for the number of selected leading eigenvectors to be rotated (S must be higher than the number of significant λ_k. For details see Ref. [2]). The authors originally called *modified* varimax criterion the maximization of (2) under $\mathbf{T}$. Here we call this the *structured* varimax (s-varimax) rotation [4].

The outcome of this rotation in the eigenvectors $\mathbf{e}^*$ is illustrated in Fig. 1(c). They are now pairwise associated to a single oscillatory mode. Since this is a phase-coherent scenario, where each oscillator has an unimodal phase dynamics, they are also pairwise associated to each PS cluster, allowing their unique identification. For example, oscillators $j = 1, 2$ share the same oscillatory modes, and so $\mathbf{e}_{1,2}^*$ reflects this shared "skeleton" (i.e., the simple structure is imposed on the remaining $2 \times m$ block whose components are now near to zero, because it should correspond to the different oscillatory behavior of oscillators $j = 3, 4$). The respective representations of the nonshared oscillatory modes of oscillators $j = 3, 4$ are now split respectively into the eigenvectors $\mathbf{e}_{3,4}^*$ and $\mathbf{e}_{5,6}^*$. In accordance, the modified variances [Fig. 1(a), blue squares] show a single leading $\lambda_{1,2}^*$ pair associated with one strong oscillatory mode (the shared mode of $j = 1, 2$) and two other pairs ($\lambda_{3,4}^*$ and $\lambda_{5,6}^*$) representing the two other modes of approximately the same "power" (from each $j = 3$ and $j = 4$).

Next (Sec. II B), we review the matrix formulation for this approach [5], which leads to the generalization to the family of orthomax rotations.

B. Structured rotations: Generalization to the orthomax family

In devising a matrix formulation for Groth and Ghil's s-varimax, Portes and Aguirre [4] generalized the concept of structured rotations to the orthomax family, from which the s-varimax is a special case. Henceforth, we will refer to this family as s-orthomax. Let $\mathbf{s}_{1,M} = (1, \ldots, 1)$ be the sum operator of order $\mathbb{R}^{1 \times M}$, $\mathbf{I}_D$ be the identity matrix of order $\mathbb{R}^{D \times D}$, and call $\mathbf{C} = (\bar{b}_{dk}^2) \in \mathbb{R}^{D,S}$. The authors defined the *structural* operator $\mathbf{\Upsilon} = \mathbf{s}_{1,M} \otimes \mathbf{I}_D \in \mathbb{R}^{D,DM}$, which allowed them to rewrite (1) in matrix form as

$$\mathbf{C} = \mathbf{\Upsilon}(\mathbf{B} \odot \mathbf{B}), \quad (3)$$

where $\otimes$ and $\odot$ are the Kronecker (direct) and the Hadamard-Schur (element-wise) products, respectively. Finally, by defining the symmetric idempotent matrix of order $\mathbb{R}^{D \times D}$

$$\mathbf{M} = \mathbf{I}_D - (\gamma/D)\mathbf{s}^T\mathbf{s}, \quad (4)$$

the matrix formulation of (2) and its generalization to the s-orthomax family are expressed by the criterion

$$Q(\mathbf{B}) = \tfrac{1}{4}\mathrm{tr}\,\mathbf{C}^T\mathbf{M}\mathbf{C}, \quad (5)$$

and its respective gradient projection

$$\mathbf{G} \doteq \mathbf{E}^T\frac{dQ}{d\mathbf{B}} = \mathbf{E}^T[\mathbf{B} \odot (\mathbf{\Upsilon}^T\mathbf{M}\mathbf{\Upsilon}\mathbf{B}^2)]. \quad (6)$$

The structured rotation can then be accomplished by setting $\gamma = 0$ for s-quartimax, $\gamma = 1/2$ for s-biquartimax, $\gamma = 1$ for Goth and Ghil's s-varimax, and $\gamma = D/2$ for s-equamax in (4).

Note that the parameter D in definition (4) corresponds to the total number of trajectory matrices that were concatenated to form the augmented trajectory matrix $\mathbf{X}$, and so correspond to the number of measured time series. In the single-variable approach [4] $D = J$, because only one time series is used to represent each dynamical system. As a consequence, the s-equamax and the s-varimax are equivalent in the context of *two* coupled dynamical systems: $\gamma = D/2 \equiv J/2 = 1$. However, in the original Groth and Ghill's approach [2], these two rotations may not be equivalent when $J = 2$, since there is no restriction for the number of measured time series for each dynamical system, and so $D \geqslant J$).

We call the attention for another two complementary results from Ref. [4], which will guide the discussion of the new results presented here. First, the s-varimax (structured) and the original (nonstructured) varimax are equivalent in the scenario of phase-coherent dynamics. Hence, the use of a structured rotation is pertinent only in more complex, multimodal, scenarios. As a consequence, we will focus here on the numeric scenario of noncoherent oscillators, specifically on coupled Rössler oscillators with intrinsic chaotic funnel regime (see Sec. III A).

Second, for noncoherent dynamics, the application of the original varimax rotation is equivalent to no rotation at all (i.e., only the s-varimax is able to allow their pairwise association with each oscillatory mode). As discussed later, our results will show surprisingly similar behavior for the structured s-equamax.

III. METHOD

A. Numeric experiment layout

Our focus is the impact of different s-orthomax on M-SSA, and hence we consider the scenario of two coupled Rössler system in the funnel (nonphase coherent or multimodal) regime—since for unimodal (phase coherent) systems, the classic varimax is sufficient and there is no necessity of the structured one [5]. This is a benchmark dynamical system that has been used to investigate the M-SSA and so allows one to build on knowledge gathered from previous studies in the literature [2,4,5,10].

The study rationale is the characterization of synchronization dynamics for an increasing coupling strength C. Consider a chain of $J = 2$ coupled Rössler systems [20]:

$$\dot{x}_j = -\omega_j y_j - z_j,$$
$$\dot{y}_j = \omega_j x_j + a y_j + C(y_{j+1} - 2y_j + y_{j-1}),$$
$$\dot{z}_j = 0.1 + z_j(x_j - 8.5). \quad (7)$$

The individual natural frequencies are $\omega_j = \omega_1 + \Delta\omega(j - 1)$, and the index $j = 1, \ldots, J$ being the position in the chain. Free boundary conditions are assumed. The coupling strength is C [not to be confounded with the matrix $\mathbf{C}$ in (3)]. With $a = 0.28$, we set the natural (uncoupled) dynamical behavior of the oscillators to the non-phase-coherent (funnel) regime. For each 200 values of the coupling strength $C \in [0, 0.2]$

system (7) is simulated for $t_{\text{sim}} = 1.2 \times 10^4$ with integration step $h = 0.01$ and then sampled with $t_s = 0.07$. After removing the initial transient ($t_{\text{tran}} = 2 \times 10^3$), the working data have a total time length $T = 1 \times 10^4$. These data were used for the straightforward synchronization analysis metrics (see Sec. III B), implying $N \approx 1.42 \times 10^5$ data points. Far fewer data points are required for the M-SSA. Then, for this analysis, the working data for this analysis were the original ones decimated by 5, yielding an effective sampling time $t_s = 0.35$ and $N \approx 2.8 \times 10^4$ data points. In view of this, the M-SSA window width or embedding dimension was set to $m = 30$ in order to embrace approximately two oscillatory cycles.

The M-SSA is then performed with the leading 20 eigenvectors $\mathbf{e_k}$ for each s-orthomax rotation: s-quartimax ($\gamma = 0$), s-biquartimax ($\gamma = 1/2$), s-varimax ($\gamma = 1$), and s-equamax ($\gamma = D/2$). The scaling $\lambda_k^{1/2} \mathbf{e_k}$ was used to determine the rotation matrix (a strategy to avoid "over-rotation" [2]). A second step is made to investigate the M-SSA robustness against noise given the chosen rotation. This is done by adding Gaussian white noise of the same variance as the original data.

Under this experimental design, we first present the results for the multivariable approach [2] (Sec. IV A). Since the three state variables x, y, and z are used to build the full augmented trajectory matrix $\mathbf{X}$, for brevity we will use the notation $\mathbf{X}_{xyz}$ to refer to this approach. Then, the results for the single-variable approach [4] with the best observable y are shown in Sec. IV B, and the notation $\mathbf{X}_y$ is used.

B. Straightforward synchronization analysis

The motivation for using some "standard" tools for phase synchronization analysis [21] is twofold: first, to provide a complementary perspective of the synchronization process as characterized by the different approaches (rotations) with the M-SSA and, second, they will support a broader discussion for a wider audience, more familiar with those metrics.

Classical methods for phase synchronization characterization are often system dependent, the main difficulty regarding a suitable way to estimate or define an instantaneous phase [21]. Here the instantaneous phases are estimated through a Poincaré section as

$$\phi(t) = 2\pi \frac{t - t_k}{t_{k+1} - t_k} + 2\pi k, \quad t_k \leqslant t < t_{k+1}, \quad (8)$$

where t_k is the time of the kth crossing, which are through the maxima of the y time series (and so been equivalent to Poincaré sampling at a differential embedding). Through this operational definition, the regime of phase synchronization can be quantified in three different ways. The first one is by the phase-locking condition: a "stronger" condition of PS, defined by a bounded phase difference $\Delta\phi(t) = |m\phi_1(t) - n\phi_2(t)| \leqslant$ const. Second, the synchronization "quality" regarding this phase difference can be estimated by the statistics [21] $S_{1,2} = \sin^2[(\phi_2(t) - \phi_1(t))/2]$. If the phases are equal, then the time average will be $\langle S_{1,2} \rangle = 0$. If they differ by π, then $\langle S_{1,2} \rangle = 1$, and $\langle S_{1,2} \rangle$ is 0.5 for uncorrelated phases. The third is the frequency entrainment condition $\Delta\Omega = \|\Omega_2 - \Omega_1\| \approx 0$, considered as a weaker condition for PS, with the mean

observed frequencies Ω_j defined as

$$\Omega_j = \lim_{T \to \infty} \frac{\phi_j(T) - \phi_j(0)}{T}. \quad (9)$$

Finally, the difference of two trajectories in state space is quantified by the normalized average error [22]

$$e = \lim \frac{1}{T} \int_0^T \frac{1}{\mathcal{D}} \|\vec{x}_2(t) - \vec{x}_1(t)\| dt, \quad (10)$$

where $\mathcal{D} = \max(\|\vec{x}_2(t) - \vec{x}_1(t)\|)$ is maximum distance in the state space. A value $e = 0$ implies in complete synchronization.

IV. RESULTS

A. Full multivariable approach

We first consider the impact of the different s-orthomax rotations on the M-SSA ability to characterize PS through the $\mathbf{X}_{xyz}$ trajectory matrix singular spectrum, Fig. 2.

The s-equamax is not only unable to show the underlying PS clustering structure, Figs. 2(e) and 2(j), but the corresponding eigenspectrum is qualitatively identical to the one obtained with *no* rotation at all [Figs. 2(a) and 2(e)]. On the other hand, the identification of an underlying PS clustering structure is accomplished by the other three s-orthomax rotations s-quartimax, s-biquartimax, and s-varimax. Henceforth we focus on this subset, which we refer as the s-QBV rotations.

Those findings suggest that only the three s-QBV rotations could be useful to the M-SSA. However, they yield remarkably different results in the funnel regime scenario, with the following four features. First, despite the fact that the high diffusive (noncoherent) phase of the funnel regime does not allow for a sharp value of coupling strength C_{PS} for the PS onset, the *range* of values for which PS emerges is quite different for each of those three rotations, with a clear shift to higher values of the coupling strength by increasing γ [Figs. 2(b)–2(d)]. Second, the high level of additive Gaussian noise makes this shift even stronger [Figs. 2(g)–2(i)], suggesting that the s-varimax is not so robust to noise regarding the identification of PS *onset* as previously believed in the literature [2,4] (but still much more robust than the straightforward synchronizaiton analysis, not shown). Third, the auxiliary PS metrics (Fig. 3) identified a PS regime for $C \geqslant C_2 \approx 0.1659$, and the M-SSA agrees with that result *regardless* of the specific s-QBV rotation applied.

Finally, note that even the high level of noise was not able to compromise the M-SSA characterization of PS for this range $C \geqslant C_2$. By this point of view, the M-SSA is *extremely* robust to additive Gaussian noise regardless of the s-QBV rotation applied.

For a deeper investigation, we consider now the M-SSA eigenvectors $\mathbf{e}_k$, Fig. 4. Three values of the coupling strength were selected, given a "stable" fingerprint of PS onset in the singular spectra for each s-QBV rotation: $C_{\text{q}} \approx 0.1050$, $C_{\text{b}} \approx 0.1149$, and $C_{\text{v}} \approx 0.1301$—those values were chosen by observing a large and stable increase of the leading pair of singular values $\lambda_{1,2}^*$ in Fig. 2 (left panel) and are highlighted by the doted vertical lines. Another two reference values were taken (see dashed vertical lines): at $C_1 \approx 0.0895$, which is prior to any sign of PS, and at $C_2 \approx 0.1659$, a value for which
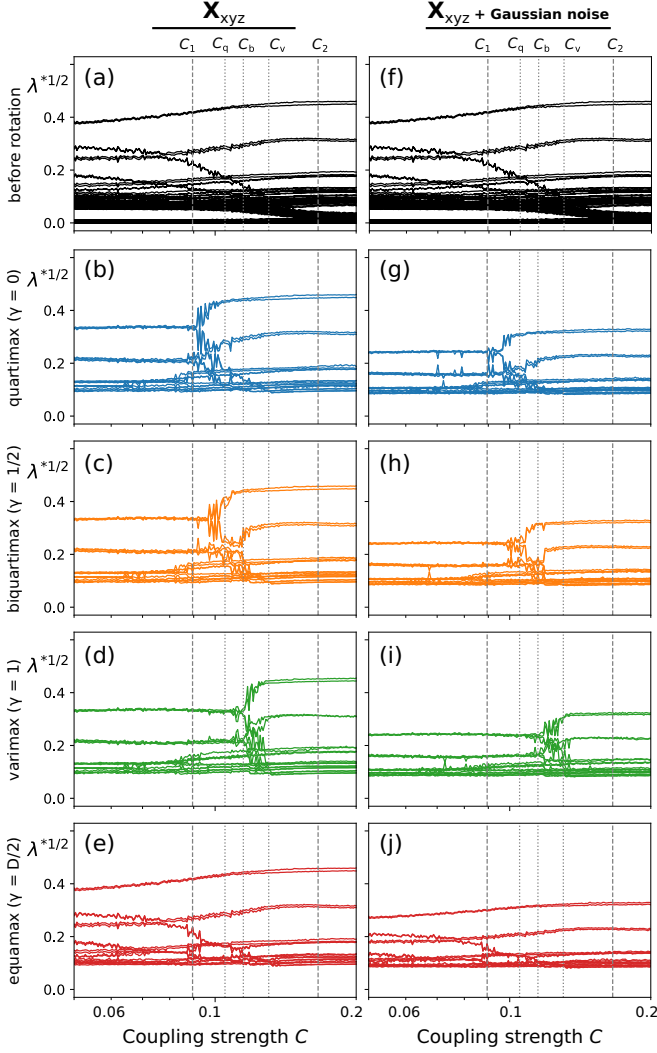
FIG. 2. Multivariable approach: Impact of the different s-orthomax rotations on the M-SSA characterization of chaotic phase synchronization for an increasing coupling strength C. Dotted vertical lines correspond to the earlier more consistent fingerprint of PS as suggested by the use of s-quartimax ($C \approx C_q$), s-biquartimax ($C \approx C_b$), and s-varimax ($C \approx C_v$). The first dashed vertical line corresponds to the absence of any PS signature ($C \geqslant C_1$). The second one corresponds to the PS onset ($C \geqslant C_2$) as identified by the auxiliary PS metrics in Fig. 3. Results for both noise free data (left panel) and data with additive Gaussian noise (right panel).
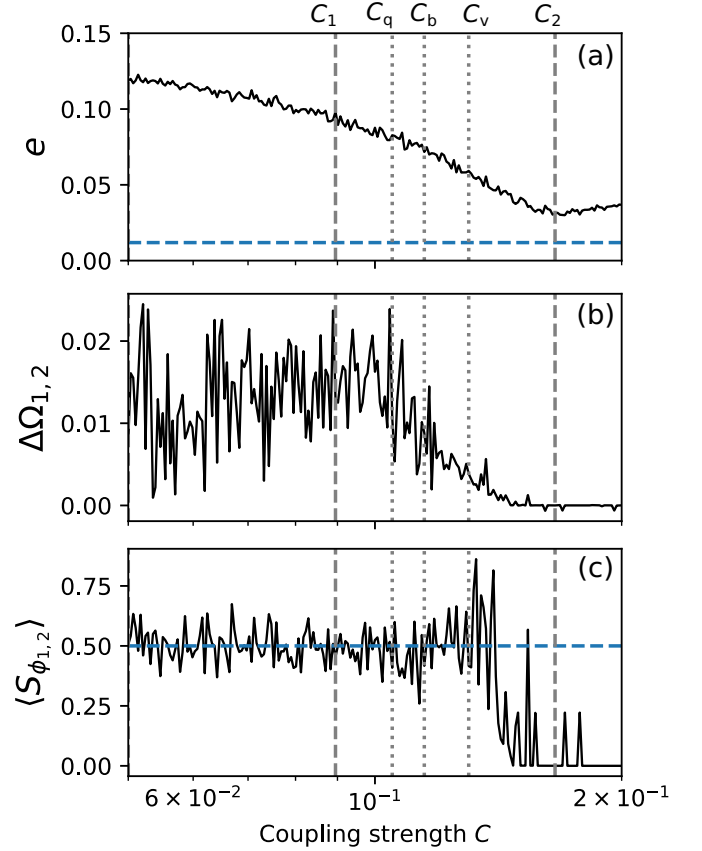

FIG. 3. Straightforward synchronization analysis for $J = 2$ coupled and detuned Rössler oscillators with intrinsic chaotic funnel dynamics. (a) Normalized average synchronization error of the trajectories (horizontal dashed line corresponds to 10% of the initial error, i.e, for $C = 0$). (b) Mean observed frequencies mismatch mod 2π. (c) "Quality" of PS as estimated by the $\langle S_{1,2} \rangle$ statistics. Vertical lines are the same as in Fig. 2.

the auxiliary PS metrics (Fig. 3) identified a PS regime. For the following discussion, we stress here that some features related to the s-varimax are already known [2,4], and the main goal of the present work is to investigate the completely unknown effects related to the remaining s-orthomax rotations.

Figure 4 shows that several oscillatory modes were identified, as captured by the eigenvectors structure [compare with Figs. 1(b) and 1(c)]. This is expected due to the high diffusive phase of the funnel regime, implying at a multimodal oscillatory dynamics [2,4]. The specific way the *structure* of these eigenvectors change due to the specific rotation (and coupling strength) illuminates the underlying mechanism for the previously shown success, or failure, of the s-orthomax

rotations regarding PS characterization through the eigenvalues λ_k^*. This can be seen in the following three features. First, *before* any sign of PS onset ($C = C_1$) the s-QBV rotations successfully associate the eigenvectors with one (and only one) Rössler oscillator and then providing evidence that no oscillatory mode is being shared by them (no fingerprint of the PS regime). This structure contrasts largely with the full mixture seen before rotation and with the s-equamax. So the s-equamax is simply not able to find the proper rotation to dissociate the eigenvectors. Second, how efficiently the s-QBV perform is quite different. The s-varimax is the most efficient, being able to split the eigenvectors for larger values of the coupling strength (C_1 to C_v). It is followed by the s-biquartimax (C_1 to C_b) and then by the less-efficient rotation s-quartimax. These results can be expressed through an "effectiveness rank" s-varimax ▷ s-Bivarimax ▷ s-quartimax (as highlighted by the increasingly wider light green rectangles). That is the underlying mechanism for the different PS onset identification by each s-QBV rotation. Specifically, since each $\mathbf{e}_k$ pair is uniquely associated with one oscillatory mode, those PS onsets are related to the first oscillatory modes that start to be *shared* (by the Rösslers oscillators), as perceived by the different s-QBV rotations. Finally, when the coupling
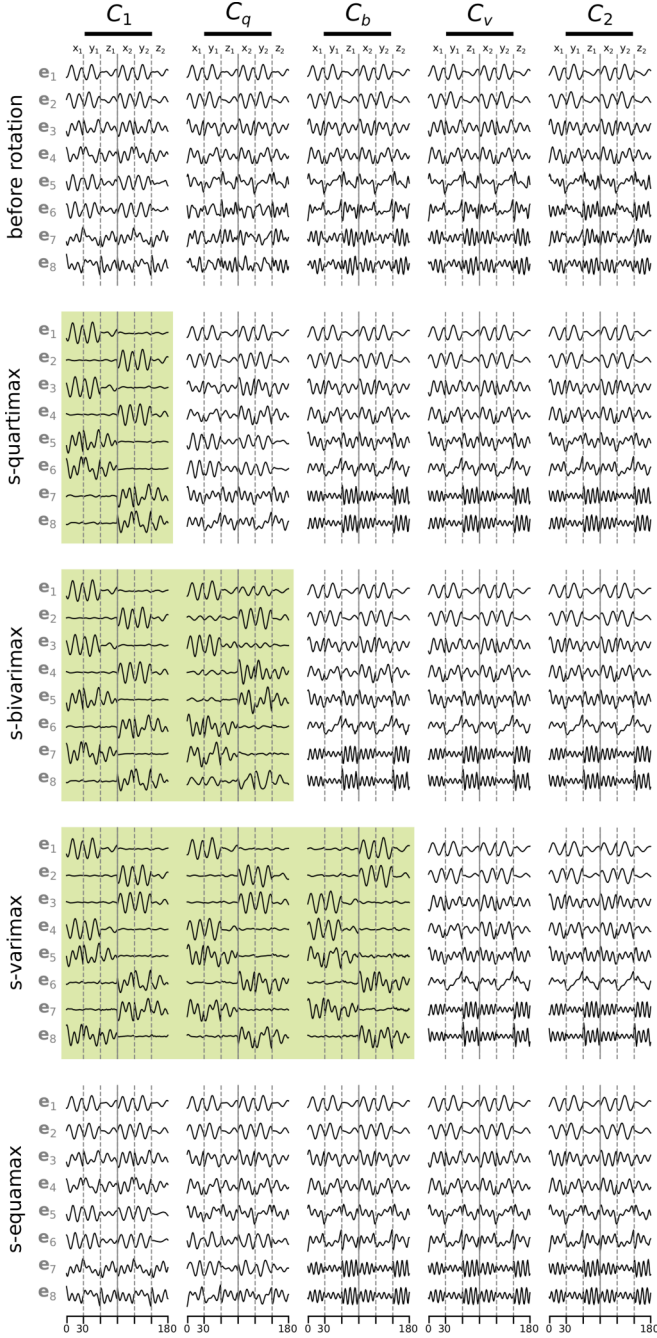
FIG. 4. M-SSA leading eight eigenvectors $\mathbf{e}_k$ for the multivariable approach. The s-QBV rotations have different abilities to associate the $\mathbf{e}_k$ pairs to each Rössler oscillator, as highlighted by the light green rectangles. The selected coupling strength values correspond to the vertical lines in Fig. 2.

strength $C = C_2$ is sufficiently large to unambiguously allows PS characterization through the locking of the estimated phases $\Delta\phi_{1,2} \approx 0$ (as well as by the other auxiliary metrics, Fig. 3), all the three s-QBV rotations agree with a complete sharing of oscillatory modes (Fig. 4, rightmost panel) and so characterizing a well-established PS regime.

But *what is the physical or dynamical interpretation for the different PS onsets?* To answer this we investigate the instantaneous phase difference $\Delta\phi/2\pi$, computed for the five selected
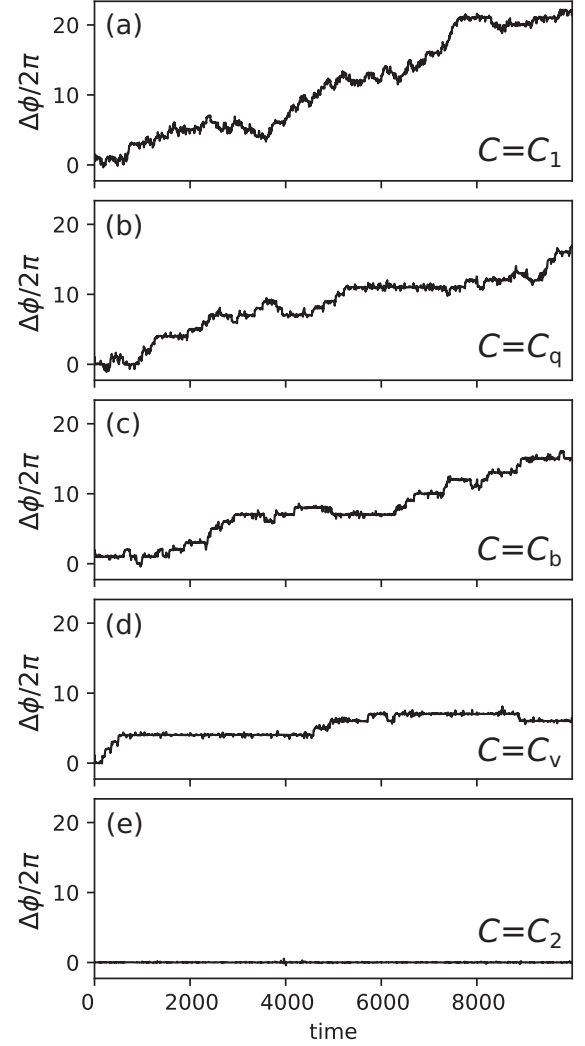

FIG. 5. Instantaneous phase difference, corresponding to the five selected coupling strengths $C \in \{C_1, C_q, C_b, C_v, C_2\}$. (a) A single small plateau (i.e., constant phase difference). Larger and more consistent plateaus are found for (b) $C = C_q$ and (c) $C = C_b$, which represent more episodes of PS dynamics. This is a signature of intermittent PS regime. (d) At $C = C_v$ the PS is even more consistent, and, finally, at (e) $C = C_2$ a full PS regime is achieved.

coupling strengths, Fig. 5. A plateau $\Delta\phi/2\pi \approx$ const implies PS. One sees that the number or the consistence (width) of plateaus increases by increasing the coupling strength. Putting in other words, at $C = C_q, C_b$ there is a regime of intermittent PS, with several phase slips. Hence, there were *episodes* of oscillatory modes sharing. However, these were not "strong" (i.e., consistent along time) enough to avoid the highly efficient s-varimax to find a rotation to dissolve the mixture effect on the eigenvectors. Then, no fingerprint for a PS regime was captured by the M-SSA with the s-varimax: See singular values at Fig. 2(d) and eigenvectors at the fourth row of Fig. 4 (under the light green rectangle). Only at the more consistent PS regime ($C = C_v$), Fig. 5(d), the sharing of modes became so consistent in time that the s-varimax is not able to find a rotation to unmix the eigenvectors. Then the M-SSA characterizes the PS onset near $C = C_v$. A similar
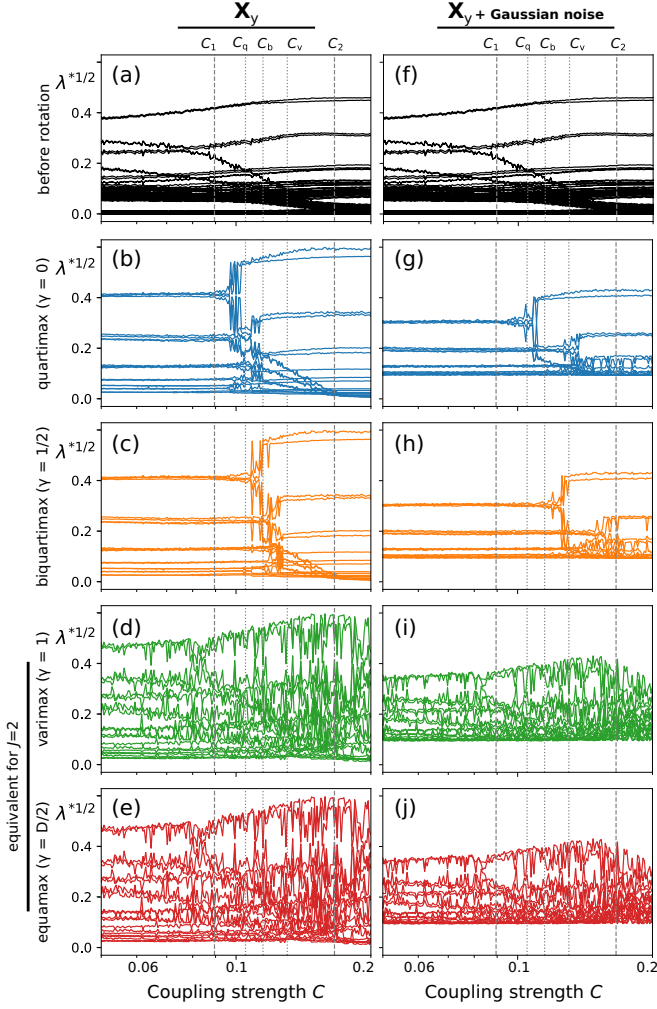
FIG. 6. Single-variable approach: Impact of the different s-orthomax rotations on the M-SSA characterization of chaotic phase synchronization for an increasing coupling strength C. Vertical line correspond to the ones in Fig. 2. Note that for $J = 2$ coupled systems, $\gamma = D/2 = 1$ in the single-variable approach and the s-equamax and s-varimax are equivalent.

argument can be applied to the s-quartimax and s-biquartimax. They progressively need a more consistent PS regime in order to not be able to unmix the eigenvectors. Then the less-efficient s-quartimax is able to characterize a less-established PS regime (in the sense of an intermittent PS regime).

Theoretical considerations can be made by framing the s-orthomax efficacy using the concept of *separability* [23–25]. Remember that each time series j contributes with a block $\mathbf{X}_j$ for the augmented (concatenated) trajectory matrix $\mathbf{X}$ (Sec. II A). Separability encapsulates the notion of orthogonality between the respective reconstructed state vectors (i.e., between the J segments of length m of a given row of $\mathbf{X}$). More specifically, it means that the eigentriple $(\lambda^{1/2}, \mathbf{P}, \mathbf{E}^T)$ from the decomposition of $\mathbf{X}$ corresponds to the union of the ones obtained by the isolated decomposition of each subtrajectory matrix $\mathbf{X}_j$. The rotation of eigenvectors aims at solving the problem of *weak* separability, where there is an "approximate" orthogonality in the original data. A higher
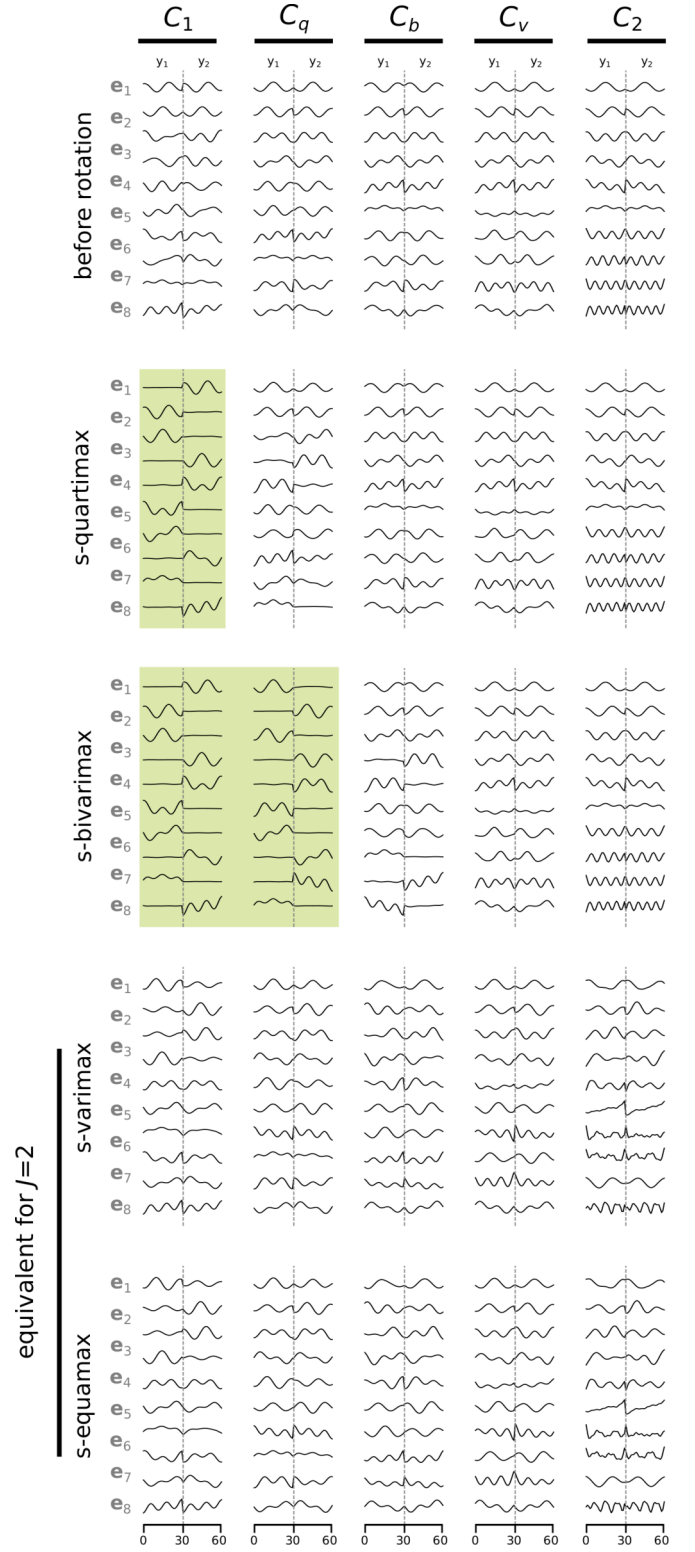

FIG. 7. M-SSA leading eight eigenvectors $\mathbf{e}_k$ for the single-variable approach. As in the multivariable approach (Fig. 4), the s-quartimax and s-biquartimax have different abilities to associate the $\mathbf{e}_k$ pairs to each Rössler oscillator (highlighted by the light green rectangles). Since $\gamma = 1$ stands for both the s-varimax and s-equamax in this context with $J = 2$ systems, the results are equivalent. The selected coupling strength values are the same as in Fig. 4.

degree of PS implies at lower separability due to the sharing of oscillatory modes. Since the varimax is the most-efficient rotation of factor analysis, it is able to find a rotation to convey a simple structure for a weaker separability (higher level of PS) than the other rotations. An in-depth discussion of separability theory for one-dimensional time series can be found in Ref. [25].

B. Single-variable approach

The results with the best observable y are shown in Figs. 6 and 7 (singular values and eigenvectors, respectively). The vertical lines are the same as in the previous analysis through the full multivariable approach. In this context, with $J = 2$ oscillators and one single time series for each one, $\gamma = 1$ implies in both the s-equamax and s-varimax and hence their results are equivalent.

The expected increased resolution of the s-varimax in single-variable approach [4] was now achieved with the s-quartimax and s-biquartimax, as seen for both the clean data and noisy data in Figs. 6(b), 6(c), 6(g), and 6(h) (note that the vertical scale is the same as in Fig. 2). The s-equamax is again not able to find a proper rotation, but it is not equivalent to the results before rotation as in the case of the full multivariable M-SSA. This is seen in both singular values, Figs. 6(e) and 6(j), and eigenvectors, Fig. 7 (bottom). Here one notices that the presence of noise imposes a larger shift for the PS onset characterization toward higher values of the coupling strength [Figs. 6(b) and 6(g) and Figs. 6(c) and 6(h)] as compared with the multivariable approach. Besides that, the *range* for PS onset with clean data is similar to the ones obtained from $\mathbf{X}_{xyz}$.

V. CONCLUSION

Multivariate singular spectrum analysis, enhanced by Groth and Ghil's structured varimax (s-varimax) rotation [2,5], is an increasingly widely utilized technique to investigate synchronization phenomena in diverse natural [3,8] and numerical scenarios [10,11]. It provides a deep characterization of phase synchronization with no necessity of *a priori* phase estimate or definition. In factor analysis, it is known that the varimax is the most-efficient rotation criterion (in the orthomax family) to achieve a simple structure of a factor matrix [12,15]. Hence, the varimax was the natural choice for the seminal modified (structured) Groth and Ghil's version do deal with PS characterization in the context of coupled dynamical systems. Here the results for the first systematic investigation of the *structured* versions of the other orthomax rotations [5] in the context of a multimodal system are five-fold:

(i) The s-orthomax rotations are not equivalent. Indeed, the useful rotations are restricted to the structured quartimax, biquartimax, and varimax (s-QBV).

(ii) The s-QBV subset has different performances to achieve the separation of eigenvectors between different systems, with an "effectiveness rank" s-varimax ▷ s-Bivarimax ▷ s-quartimax.

(iii) This rank is related to the strength of PS. Hence, while the s-varimax could be used as a test for a more consolidated PS regime, the s-quartimax seems to be the best choice if the goal is the characterization of a faint, less developed, and intermittent PS regime.

(iv) Additive Gaussian noise slightly overshoots the identification of PS *onset*. This effect is stronger in the single-variable approach than in the multivariable one.

(v) In the single-variable approach, $J = 2$ oscillators implies in the equivalence among the s-varimax and s-equamax (because $\gamma = D/2 \equiv J/2 = 1$). As a consequence, in *this* specific context the choice $\gamma = 1$ yields no useful results. It is worth noticing that this was acknowledged in Ref. [4]; the authors stated that ". . . if $J = 2$ in the single-variable M-SSA . . . the structured varimax rotation (SRV) fails to separate the rotated eigenvectors." Then the authors found, empirically, that the $\gamma = 2/3 \approx 0.66$ gave an appropriate rotation. Indeed, we found good rotations for values of γ near to 1 (e.g., 0.99, results not shown here). However, we restrict the presentation of results to the γ values corresponding to this study scope: the orthomax family ($\gamma \in \{0, 1/2, 1, D/2\}$).

We expect that the results provided here could be used in two ways: first, by providing a choice for the researcher in adjusting the desired sensitivity to establish a PS regime through time-series analysis, in accordance with his or her specific experimental scenario under investigation. For example, by applying the s-quartimax for a earlier identification of PS onset. However, we stress here that discussing just sensitivity without specificity is dangerous [6], and this complementary point of view is left for further investigation.

Second, the *joint* application of the s-QBV rotations could provide tests for PS in more complex scenarios, given that they agree when this regime is more developed or consolidated, and disagree when it becomes intermittent. Those ideas could be employed at the implementation of specific sensors, being focused on more sensitivity for PS onset characterization or more reliability in discern very-weak to moderate PS levels and intermittent regimes.

[1] M. Ghil, M. R. Allen, M. D. Dettinger, K. Ide, D. Kondrashov, M. E. Mann, A. W. Robertson, A. Saunders, Y. Tian, F. Varadi, and P. Yiou, Advanced spectral methods for climate time series, Rev. Geophys. **40**, 31 (2002).

[2] A. Groth and M. Ghil, Multivariate singular spectrum analysis and the road to phase synchronization, Phys. Rev. E **84**, 036206 (2011).

[3] A. Groth and M. Ghil, Synchronization of world economic activity, Chaos **27**, 127002 (2017).

[4] L. L. Portes and L. A. Aguirre, Enhancing multivariate singular spectrum analysis for phase synchronization: The role of observability, Chaos **26**, 093112 (2016).

[5] L. L. Portes and L. A. Aguirre, Matrix formulation and singular-value decomposition algorithm for structured varimax rotation

in multivariate singular spectrum analysis, Phys. Rev. E **93**, 052216 (2016).

[6] A. Groth and M. Ghil, Monte Carlo singular spectrum analysis (SSA) revisited: Detecting oscillator clusters in multivariate datasets, J. Clim. **28**, 7873 (2015).

[7] K. Pukenas, Detecting phase synchronization in coupled oscillators by combining multivariate singular spectrum analysis and fast factorization of structured matrices, J. Vibroengineering **16**, 2624 (2014).

[8] Y. Feliks, A. Groth, A. W. Robertson, and M. Ghil, Oscillatory climate modes in the Indian monsoon, north Atlantic, and tropical pacific, J. Clim. **26**, 9528 (2013).

[9] A. Groth, Y. Feliks, D. Kondrashov, and M. Ghil, Interannual variability in the north Atlantic ocean's temperature field and its association with the wind stress forcing, J. Clim. **30**, 2655 (2017).

[10] L. L. Portes and L. A. Aguirre, Impact of mixed measurements in detecting phase synchronization in networks using multivariate singular spectrum analysis, Nonlinear Dynam. **96**, 2197 (2019).

[11] L. A. Aguirre, L. L. Portes, and C. Letellier, Observability and synchronization of neuron models, Chaos **27**, 103103 (2017).

[12] H. F. Kaiser, The varimax criterion for analytic rotation in factor analysis, Psychometrika **23**, 187 (1958).

[13] C. A. Bernaards and R. I. Jennrich, Gradient projection algorithms and software for arbitrary rotation criteria in factor analysis, Educ. Psychol. Meas. **65**, 676 (2005).

[14] R. I. Jennrich, A simple general procedure for orthogonal rotation, Psychometrika **66**, 289 (2001).

[15] H. F. Kaiser, An index of factorial simplicity, Psychometrika **39**, 31 (1974).

[16] L. L. Thurstone, Multiple factor analysis, Psychol. Rev. **38**, 406 (1931).

[17] M. B. Richman, Rotation of principal components, J. Climatol. **6**, 293 (1986).

[18] F. Takens, Detecting strange attractors in turbulence, in *Dynamical Systems and Turbulence, Warwick 1980*, Vol. 898, edited by D. Rand and L. S. Young (Springer, Berlin, 1981), pp. 366–381.

[19] D. Broomhead and G. P. King, Extracting qualitative dynamics from experimental data, Physica D **20**, 217 (1986).

[20] G. V. Osipov, A. S. Pikovsky, M. G. Rosenblum, and J. Kurths, Phase synchronization effects in a lattice of nonidentical Rössler oscillators, Phys. Rev. E **55**, 2353 (1997).

[21] G. V. Osipov, J. Kurths, and C. Zhou, in *Synchronization in Oscillatory Networks*, 1st ed., edited by H. Haken, Springer Series in Synergetics (Springer, Berlin, 2007), p. 370.

[22] I. Sendiña-Nadal and C. Letellier, Synchronizability of nonidentical weakly dissipative systems, Chaos **27**, 103118 (2017).

[23] N. Golyandina, Particularities and commonalities of singular spectrum analysis as a method of time series analysis and signal processing, arXiv:1907.02579.

[24] N. Golyandina, A. Korobeynikov, A. Shlemov, and K. Usevich, Multivariate and 2D extensions of singular spectrum analysis with the Rssa package, J. Stat. Softw. **67**, 1 (2015).

[25] N. Golyandina, V. Nekrutkin, and A. Zhigljavsky, *Analysis of Time Series Structure*, C&H/CRC Monographs on Statistics & Applied Probability (Chapman & Hall/CRC, London, 2001), Vol. 90.